

# Structure, electronic properties and magnetic transition in manganese clusters

Mukul Kabir and Abhijit Mookerjee

Unit for Nanoscience and Technology, S.N. Bose National Center for Basic Sciences,  
JD Block, Sector III, Salt Lake City, Kolkata 700 098, India

D. G. Kanhere

Department of Physics and Center for Modeling and Simulation,  
University of Pune, Pune - 411 007, India

(Dated: September 6, 2017)

We systematically investigate the structural, electronic and magnetic properties of  $Mn_n$  clusters ( $n = 2-20$ ) within the *ab-initio* pseudopotential plane wave method using generalized gradient approximation for the exchange-correlation energy. A new kind of icosahedral structural growth has been predicted in the intermediate size range. Calculated magnetic moments show an excellent agreement with the Stern-Gerlach experiment. A transition from ferromagnetic to ferrimagnetic  $Mn-Mn$  coupling takes place at  $n = 5$  and the ferrimagnetic states continue to be the ground states for the entire size range. Possible presence of multiple isomers in the experimental beam has been argued. No signature of non-metal to metal transition is observed in this size range and the coordination dependence of  $d$ -electron localization is discussed.

PACS numbers: 75.75.+a, 36.40.Cg, 61.46.Bc, 73.22.-f

## I. INTRODUCTION

The search for magnetic behavior in the transition metal clusters is motivated largely by the desire to understand how magnetic properties change in the reduced dimension. This is a question of considerable technological importance. Several unexpected magnetic orderings have already been reported in the reduced dimension. This ranges from the prediction of net magnetic moment in clusters of nonmagnetic (Rh, Ref. 1) or antiferromagnetic (Cr, Ref. 2 and Mn, Refs. 3 and 4) bulk materials to the enhancement in magnetic moment in clusters of ferromagnetic metals (Fe, Ref. 5 and Co, Ref. 6).

Manganese clusters are particularly interesting among all 3d transition metal elements due to the  $4s^2$ ,  $3d^5$  electronic configuration in Mn atoms. Because of the filled  $4s$  and half-filled  $3d$  shells and the large energy gap  $\sim 8$  eV between these levels and as well as due to the high  $4s^23d^5 \rightarrow 4s^13d^6$  promotion energy of 2.14 eV<sup>7</sup>, Mn atoms do not bind strongly. As a result,  $Mn_2$  is a weakly bound van der Waals dimer with reported bond dissociation energy ranging from  $0.1 \pm 0.1$  to  $0.56 \pm 0.26$  eV depending upon the different method of analysis<sup>8,9,10,11</sup>. This weak Mn–Mn bonding has been demonstrated through the photodissociation experiments for  $Mn_n^+$  ( $n \leq 7$ ) cluster cations<sup>11,12</sup>. Consequently, the bulk  $\alpha$ -Mn, which has a very complex lattice structure with 58 atoms in the unit cell, has the lowest binding energy among all the 3d transition metal elements.

Magnetic properties of manganese clusters are rather unusual. According to Hund's rule, the half-filled localized 3d electrons give rise to large atomic magnetic moment of  $5 \mu_B$ . An early electron spin resonance (ESR) study suggested a magnetic moment of  $5 \mu_B/\text{atom}$  for very small Mn clusters<sup>13</sup>. However, Stern-Gerlach (SG) molecular beam experiments on  $Mn_{5-99}$  clusters by

Knickelbein recently revealed the net magnetic moments ranging from  $0.4$  to  $1.7 \mu_B/\text{atom}$ <sup>3,4</sup>. This differs both from the ferromagnetic (FM) small clusters and from the antiferromagnetic (AFM) bulk  $\alpha$ -Mn. This experimental results can be explained either way that the individual atomic moments are small and ordered ferromagnetically or the individual atomic moments remain large but their orientation flips from site to site i.e., they are coupled ferrimagnetically. In the SG experiment, it is important to note the relative decrease in the magnetic moment for  $Mn_{13}$  and  $Mn_{19}$ , as well as the relatively very large experimental uncertainty in the measured magnetic moment for  $Mn_7$ <sup>3,4</sup>. In the present work, we will show that the local minima for  $Mn_{13}$  and  $Mn_{19}$  arise due to their 'closed' icosahedral structures, whereas, the large experimental uncertainty ( $\pm 58\%$  of the measured value) in the magnetic moment of  $Mn_7$  is plausibly due to the production of different magnetic isomers (in addition with statistical fluctuation) in the subsequent measurements.

Earlier all electron (AE) studies<sup>14,15,16</sup> found Mn–Mn FM ordering for  $Mn_n$  ( $n > 4$ ) clusters, which, in turn, is not consistent with the SG experiment. However, Nayak *et al.* first predicted ferrimagnetic ground state for  $Mn_{13}$  with a total magnetic moment of  $33 \mu_B$ <sup>17</sup>. In consistent with the SG experiments, very recent AE studies by Parvanova *et al.*<sup>18,19</sup> ( $n = 2-9$ , 12 and 13) and Jones *et al.*<sup>20</sup> ( $n = 5$  and 6) reported ferrimagnetic ordering in  $Mn_n$  clusters. Briere *et al.*<sup>21</sup> used ultra-soft pseudopotentials (US-PP) to study the intermediate size  $Mn_n$  clusters ( $n = 13$ , 15, 19 and 23) and found icosahedral structural growth with an exception for  $Mn_{15}$ . However, their predicted magnetic moments differ widely from the experimental values. This might be attributed to the reason that the US-PP may not be appropriate in describing the transition metals with large magnetic moments. This will be discussed briefly later in the section II. Our main

motivation of this work is particularly driven by the SG experiments<sup>3,4</sup>. Here we shall investigate – (i) The structural and magnetic evolution of  $Mn_n$  clusters,  $n=2-20$ . (ii) The sudden drop in the magnetic moment at  $n=13$  and 19 and the very large experimental uncertainty in the measured magnetic moment for  $Mn_7$ , and (iii) The possible presence of isomers with different magnetic structures in the SG experimental molecular beam.

It has also been found by Parks *et al.* that the  $Mn_n$  clusters show a downward discontinuity in their reaction rate with molecular hydrogen at  $n = 16$ , and this was attributed to non-metal to metal transition in  $Mn_{16}$ <sup>22</sup>. But if this is indeed true then there should be a downward decrease in the ionization potential too. However, no such abrupt decrease has been seen in the measured ionization potential<sup>23</sup>. In the present paper, we calculate both the spin gaps to investigate this issue.

## II. COMPUTATIONAL DETAILS

The calculations are performed using density functional theory (DFT), within the pseudopotential plane wave method. We have used projector augmented wave (PAW) method<sup>24,25</sup> and Perdew-Bruke-Ernzerhof (PBE) exchange-correlation functional<sup>26</sup> for spin-polarized generalized gradient correction (GGA) as implemented in the Vienna *ab-initio* Simulation Package (VASP)<sup>27</sup>. The 3d and 4s electrons are treated as valence electrons and the wave functions are expanded in the plane wave basis set with the kinetic energy cut-off 337.3 eV. Reciprocal space integrations are carried out at the  $\Gamma$  point. Symmetry unrestricted geometry and spin optimizations are performed using conjugate gradient and quasi-Newtonian methods until all the force components are less than a threshold value 0.005 eV/Å. Simple cubic supercells are used with the periodic boundary conditions, where two neighboring clusters are kept separated by at least 12 Å vacuum space. For each size, several initial geometrical structures have been considered. To get the ground state magnetic moment we have explicitly considered *all possible* spin configurations for each geometrical structure. For transition metals with large magnetic moments, the PAW method seems to be more appropriate (as good as the AE calculations) than the US-PP approach<sup>25</sup>. The US-PP overestimates the magnetization energies and this overestimation is even more large for GGA calculations than local spin density approximation (LSDA). This is due to the fact that the GGA functionals are more sensitive to the shape of the wave functions than the LSDA functionals. However, the difference between these two methods, US-PP and PAW, are solely related to the pseudization of the augmentation charges in the US-PP approach, which can be removed by choosing very accurate pseudized augmentation function, which is then computationally expensive. For a better description see the Ref. 25 by Kresse and Joubert.

The binding energy per atom is calculated as,

$$E_b(Mn_n) = \frac{1}{n} [E(Mn_n) - n E(Mn)], \quad (1)$$

$n$  being the size of the cluster. The local magnetic moment  $\mathcal{M}$ , at each site can be calculated as,

$$\mathcal{M} = \int_0^R [\rho^\uparrow(\mathbf{r}) - \rho^\downarrow(\mathbf{r})] dr, \quad (2)$$

where  $\rho^\uparrow(\mathbf{r})$  and  $\rho^\downarrow(\mathbf{r})$  are spin-up and spin-down charge densities, respectively and  $R$  is the radius of the sphere centering the atom. For a particular cluster,  $R$  is taken such that no two spheres overlap i.e.,  $R$  is equal to the half of the shortest bond length in that cluster.

## III. RESULTS AND DISCUSSIONS

### A. Small Ferromagnetic Clusters ( $Mn_2$ - $Mn_4$ )

The  $Mn_2$  dimer is the most controversial among all the sizes we have studied. Experiments based on resonance Raman spectroscopy<sup>28</sup> and ESR<sup>29</sup> observed an AFM ground state with a bond length 3.17 Å. Experimentally the binding energy was estimated to be  $0.44 \pm 0.30$  eV/atom<sup>8,9,10</sup>. However, previous AE-DFT calculations<sup>14,16,18,19</sup>, predicted a FM state to be the ground state with much smaller bond length ( $\sim 2.60$  Å) than that of the experimental value. In agreement with these calculations, our present PAW pseudopotential calculations with PBE exchange-correlation functionals, predict a FM ground state with total spin  $10 \mu_B$  and with bond length 2.58 Å. Very small binding energy, 0.52 eV/atom, is essentially the characteristic of a van der Waals system. However, the bond dissociation energy increases by considerable amount due to the reduction of one electron from the  $Mn_2$  dimer, i.e. by creating a hole in the 4s level. As measured by the photodissociation experiment the bond dissociation ( $Mn^+ \cdots Mn$ ) energy increases to 1.39 eV for  $Mn_2^+$  cation<sup>30</sup>. We find that the bond length of  $Mn_2$  decreases monotonically as the net moment decreases. This is consistent with the physical picture that the reduction of the interatomic spacing leads to comparatively stronger overlap of the atomic orbitals which, in turn, reduces the magnetic moment. However, we find  $Mn_2$  with total moment 4 and  $6 \mu_B$  are not bound. An AF  $Mn_2$  is 0.52 eV higher in energy with bond length 2.61 Å. The present results, along with the previous AE-DFT calculations<sup>14,16,18,19</sup>, do not agree with the experimental results. This might be attributed to the fact that the density functional theory is not adequate in treating van der Waals interaction properly. However, there is no experimental results available in the gas phase  $Mn_2$  dimer and the ESR experiment was done in a rare gas matrix. Therefore, it is possible that the Mn atoms do interact with the matrix, which could stretch the bond length and could lead to the observed AFM state.

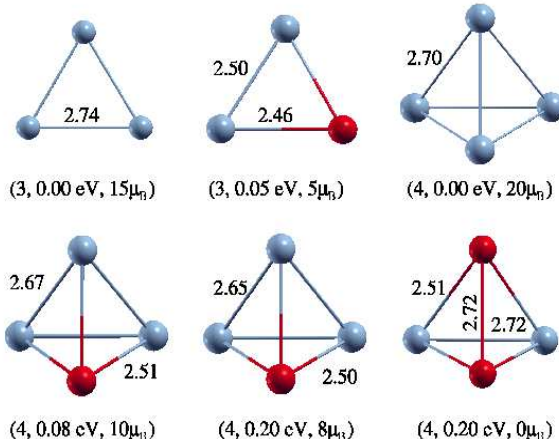


FIG. 1: (Color online). Atomic spin ordering of the ground state and low-lying isomers for  $Mn_3$  and  $Mn_4$  clusters. Numbers in the parenthesis represent number of atoms in the cluster, relative energy to the ground state and total magnetic moment, respectively. Bond lengths are given in Å. Blue (Gray) color represents up or positive and red (dark gray) represents down or negative magnetic moment. We will follow the same convention throughout.

The case of  $Mn_3$  is extremely interesting as it could have either FM or a frustrated AFM structure. We have studied triangular and linear structures. An equilateral triangular FM state with total moment  $15 \mu_B$  is found to be the ground state with bond lengths  $2.74 \text{ \AA}$  and binding energy  $0.82 \text{ eV/atom}$ . The frustrated AFM state with total moment  $5 \mu_B$  is found to be nearly degenerate with the FM ground state (lies only  $0.05 \text{ eV}$  higher in energy). This has an isosceles triangular structure with one long and two short bond lengths of  $2.50$  and  $2.45 \text{ \AA}$ , respectively (Fig.1). The resonance Raman spectra studies by Bier *et al.*<sup>28</sup> suggest the ground state to be Jahn-Teller distorted  $D_{3h}$  structure with an odd integer magnetic moment.

For the  $Mn_4$  cluster, we examined three different conformations: square, rhombus and tetrahedron. A perfect tetrahedral structure with bond lengths  $2.7 \text{ \AA}$  and binding energy  $1.18 \text{ eV/atom}$  is the ground state, where  $Mn-Mn$  coupling is FM with total moment  $20 \mu_B$  (Fig.1). Three isomers are found and all of them are tetrahedral. A ferrimagnetic state with total moment  $10 \mu_B$  is only  $0.08 \text{ eV}$  higher in energy. Another ferrimagnetic state with total moment  $8 \mu_B$  is found to be degenerate with the AF state with no net moment and they are  $0.20 \text{ eV}$  higher in energy. In all these optimal structures the distances between two similar spins ( $d_{\uparrow\uparrow}$  or  $d_{\downarrow\downarrow}$ ) are larger than those of between two opposite spins ( $d_{\uparrow\downarrow}$ ). Our results are consistent with the previous AE calculations<sup>14,16,18,19</sup>. Ludwig *et al.*<sup>31</sup> have studied  $Mn_4$  in solid silicon and observed a 21-line hyperfine pattern that not only establishes the four atoms to be equivalent, but also the total moment to be  $20 \mu_B$ . However, the present results can not directly be compared with this ex-

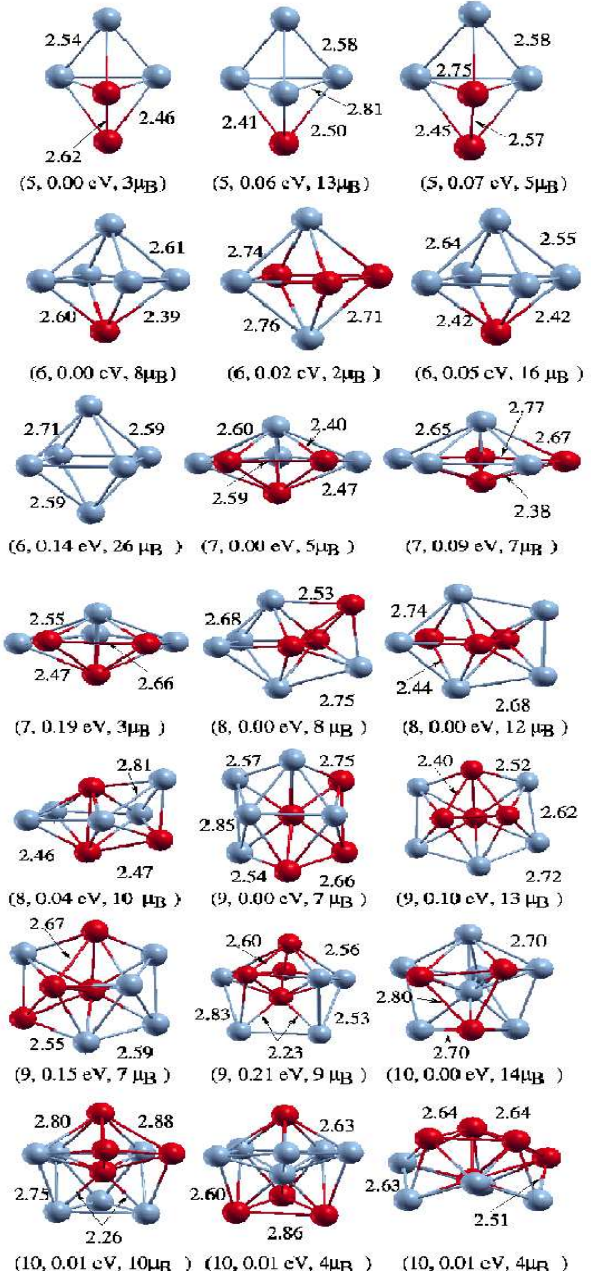


FIG. 2: (Color online). Atomic spin ordering of the ground and isomeric geometries for  $n = 5-10$ . Same ordering has been followed as in the Table I.

periment because of possible Si-Mn interaction and there is no available report of magnetic ordering for  $Mn_4$  in its gas phase.

## B. $\text{Mn}_5$ - $\text{Mn}_{10}$

As the number of atoms in the cluster ( $n$ ) increases the determination of the structural and magnetic ground state becomes a very delicate task as the number of local

minima in the corresponding potential energy surface increases exponentially with  $n$ . Therefore, more than one geometric and/or magnetic structures of comparable stability are possible. In the Fig.2 we depict the atomic and magnetic structures for the ground state as well as for the closely lying isomers for the size range  $n = 5-10$ . As it is mentioned earlier, to hit the ground state more reliably, we have studied *all possible* spin multiplicities for several geometric structures for a particular cluster size  $n$ . Calculated binding energies, relative energies, magnetic moments and two spin gaps are given in the Table I for the entire size range  $n = 2-20$ .

For the  $Mn_5$  cluster, a square pyramid and a triangular bi-pyramid (TBP) were studied. Transition in the magnetic order, from FM to ferrimagnetic, is found. A ferrimagnetic TBP is found to be the ground state with total spin  $3 \mu_B$ . The next two isomers are also ferrimagnetic in nature with total spins  $13 \mu_B$  and  $5 \mu_B$ . Both of these structures also have TBP structure and lie 0.06 and 0.07 eV, respectively, higher in energy. The next lowest energy arrangement is FM and also has a TBP structure with total spin  $23 \mu_B$  and lies 0.19 eV higher in energy. Our results are in agreement with the very recent AE calculations<sup>18,19,20</sup>. However, previously the FM ground state was predicted by both Nayak *et al.*<sup>14,15</sup> and Pederson *et al.*<sup>16</sup>. In the recent SG experiment<sup>4</sup>, magnetic moment was found to be  $0.79 \pm 0.25 \mu_B/\text{atom}$ , which is very close to our predicted value  $0.60 \mu_B/\text{atom}$  for the ground state.

We have investigated both the octahedral and the capped trigonal bi-pyramid for  $Mn_6$  cluster. A ferrimagnetic octahedral structure with total spin  $8 \mu_B$  is found to be the ground state with binding energy 1.57 eV/atom. Another octahedral ferrimagnetic isomer with total moment  $2 \mu_B$  is nearly degenerate (0.02 eV higher in energy). The next isomer is also a ferrimagnetic octahedra, which possess a total moment of  $16 \mu_B$  and lies 0.05 eV higher. The next favorable isomer is FM and has a total moment  $26 \mu_B$  and is 0.14 eV higher than the ground state. In an earlier calculation, Pederson *et al.*<sup>16</sup> predicted a FM octahedral structure with moment  $4.33 \mu_B/\text{atom}$  to be the ground state. However, in agreement with the recent AE-DFT calculations<sup>18,19,20</sup>, present calculation predicts the same ground state and isomers. Experimentally measured magnetic moment  $0.55 \pm 0.10 \mu_B/\text{atom}$ <sup>4</sup> lies between that of our predicted ground state,  $1.33 \mu_B/\text{atom}$  and the first isomer,  $0.33 \mu_B/\text{atom}$ , which are almost degenerate. It is possible that in the SG experimental beam, multiple isomers were produced such that the measured value is almost an average of the ground state and the first isomer.

We have considered pentagonal bi-pyramid (PBP), capped octahedron and bi-capped trigonal pyramid as the possible candidates for the ground state of  $Mn_7$ . The most stable configuration is a PBP structure with ferrimagnetic spin ordering, which has a total moment  $5 \mu_B$ . The next two closest isomers also have ferrimagnetic arrangements with  $7 \mu_B$  and  $3 \mu_B$  total moments

and they lie 0.09 eV and 0.20 eV higher than the ground state, respectively. Our ground state magnetic moment agrees with the earlier calculations<sup>18,19,32</sup>, though we predict isomers with different spin arrangements. However, Pederson *et al.* predicted a FM ground state<sup>16</sup>. Present ground state magnetic moment per atom exactly matches with the experimental value,  $0.72 \pm 0.42 \mu_B/\text{atom}$ <sup>4</sup>. We would like to note the rather large uncertainty here. We argue that the plausible presence of these isomers, with total moments  $7 \mu_B$  and  $3 \mu_B$  along with the ground state ( $5 \mu_B$ ), in the SG beam might lead to this high uncertainty in the measured value.

Motivated by our earlier study on  $Cu_8$ <sup>33,34</sup>, we investigated three different geometries for  $Mn_8$ , viz, capped pentagonal bi-pyramid (CPBP), bi-capped octahedron (BCO) and tri-capped trigonal bi-pyramid (TCTBP). The BCO structure with total moments  $8 \mu_B$  and  $12 \mu_B$  are found to be degenerate ground state. Another BCO structure with total moment  $10 \mu_B$  lies only 0.03 eV higher in energy. The SG cluster beam experiment has reported a magnetic moment of  $1.04 \pm 0.14 \mu_B/\text{atom}$ <sup>4</sup>, which is nearly an average of our predicted values. Therefore, our present DFT study together with the experiment in turn indicate the possible presence of these three isomers in the experimental beam with almost equal statistical weight. The optimal CPBP and TCTBP structures have total moments  $14 \mu_B$  and  $12 \mu_B$ , respectively and they lie 0.31 and 0.4 eV higher than the ground state. Parvanova *et. al.*<sup>19</sup> found CPBP structure to be the most stable, however, their predicted magnetic moment is very small,  $4 \mu_B$ , compared to both of our value and the SG experiment. Pederson *et. al.*<sup>16</sup> predicted a FM BCO structure with moment  $32 \mu_B$  as the ground state. The optimal FM structure for all the three geometrical structures have total moment  $32 \mu_B$  and lie 1.01, 0.63 and 1.17 eV higher in energy compare to their respective optimal ferrimagnetic structure, respectively for BCO, CPBP and TCTBP structures.

For the  $Mn_9$  cluster, as initial configuration we took three stable isomers found for  $Cu_9$ <sup>33,34</sup> and a capped and a centered antiprism structure. The optimal structure is a centered antiprism structure with total moment  $7 \mu_B$ , which is in very good agreement with the experimental value  $1.01 \pm 0.10 \mu_B/\text{atom}$ <sup>4</sup>. The local magnetic moment  $\mathcal{M}$  (as calculated from the Eq. 2) shows strong environment dependency due to the anisotropy in bonding. The  $\mathcal{M}$  of the highly coordinated central atom is very small,  $-0.22 \mu_B$ , whereas those of the surface atoms are quite high and lie between  $3.45$  and  $3.75 \mu_B$ . Parvanova *et al.*<sup>19</sup> have found a similar structure but with different spin configuration with total moment  $9 \mu_B$  to be the optimal structure. The next two isomers have the same geometry and have  $13$  and  $7 \mu_B$  total magnetic moment (Fig.2 and Table I). The next isomer is a bi-capped pentagonal bi-pyramid, which lies 0.21 eV higher with a total moment of  $9 \mu_B$ . The optimal capped antiprism structure lies 0.23 eV higher and has a total moment of  $7 \mu_B$ . Note that, all these structures have 5 spin-up ( $N_\uparrow$ )

atoms and 4 spin-down ( $N_\downarrow$ ) atoms.

Different tricapped pentagonal bi-pyramidal structures along with different tetra capped octahedral structures were tried as initial structures for  $Mn_{10}$ . Four isomers exist with almost the same energy. They lie within  $\sim 0.01$  eV energy (see Table I and Fig. 3). All of these have a pentagonal ring and could be derived by removing 3 atoms from a 13-atom icosahedra. Ground state has a total magnetic moment  $14 \mu_B$ , which is very close to the SG experimental value,  $1.34 \pm 0.09 \mu_B/\text{atom}$ <sup>4</sup>.

### C. Intermediate size clusters: $Mn_{11}$ - $Mn_{20}$

All the intermediate sized clusters with  $n = 11$ -20 are found to adopt an icosahedral growth pattern. The ground state structures and the few isomers along with their corresponding spin arrangements are shown in the Fig.3. An icosahedral structure without one apex atom is found to be the ground state for the  $Mn_{12}$  cluster. This structure has  $N_\uparrow = 8$  and  $N_\downarrow = 4$  spin configuration with a total moment of  $16 \mu_B$ . This value is close to the experimentally measured value of  $1.72 \pm 0.04 \mu_B/\text{atom}$ <sup>3,4</sup>. Recently Parvanova *et al.* predicted the same geometrical structure but with comparatively smaller,  $1 \mu_B/\text{atom}$ , magnetic moment<sup>19</sup>. We have found two closely lying isomers, which have the same geometrical structure with total moments  $4 \mu_B$  and  $18 \mu_B$  (Table I). Another possible icosahedral structure without the central atom lies much higher in energy.

The obvious candidates for the  $Mn_{13}$  cluster are the icosahedral, hexagonal close packed (HCP) and cuboctahedral structures. The variation of total energy as a function of the total magnetic moment is plotted in the Fig.4 for all these three conformations. The icosahedral structure is found to be the ground state with  $N_\uparrow = 7$  spin structure. The two pentagonal rings are AFM coupled for this structure (Fig.3). Consequently, the magnetic moment is found to be small,  $0.23 \mu_B/\text{atom}$ . This predicted magnetic moment is much smaller than those of its neighboring  $Mn_{12}$  and  $Mn_{14}$  clusters (Fig.6), what has been indeed predicted by the SG experiment<sup>3,4</sup>. Although, the present value is much lower than the experimental value of  $0.54 \pm 0.06 \mu_B/\text{atom}$ <sup>4</sup>. However, we have found another icosahedral isomer with magnetic moment exactly the same with the experimental value, which lies only  $0.08$  eV higher in energy (Table I). This structure also has  $N_\uparrow = 7$ . Recently, Parvanova *et al.* predicted similar magnetic ordering<sup>19</sup>. The optimal HCP and cuboctahedral structures (Fig.3) have relatively higher magnetic moments  $9 \mu_B$  ( $N_\uparrow = 7$ ) and  $11 \mu_B$  ( $N_\uparrow = 8$ ), respectively, and they lie much higher in energy,  $0.89$  eV and  $1.12$  eV, respectively. Nayak *et al.* first predicted a ferrimagnetic state for  $Mn_{13}$ . However, their predicted magnetic moment is quite high ( $33 \mu_B$ ): all the surface atoms are antiferromagnetically coupled with the central atom<sup>17</sup>.

The ground state of  $Mn_{14}$  is the first complete icos-

hedra with a single atom capping. This structure has  $N_\uparrow = 9$ , with a magnetic moment  $1.29 \mu_B/\text{atom}$ . In this structure the magnetic coupling between the two pentagonal rings is FM, which was coupled antiferromagnetically in the case of  $Mn_{13}$  and consequently, it has small magnetic moment. The next two isomers lie very close to the ground state: they lie only  $0.02$  eV and  $0.05$  eV higher and have  $1.43$  and  $1.57 \mu_B/\text{atom}$  magnetic moment, respectively. These two isomers (not shown in Fig.3) have the same  $N_\uparrow = 9$  spin structure, but with their different positional arrangement. The experimentally predicted magnetic moment,  $1.48 \pm 0.03 \mu_B/\text{atom}$ , is an average of the ground state and the two isomers (Table I), which again indicates that these isomers might be produced along with the ground state in the SG experiment.

The discrepancy between the present theoretical and experimental magnetic moment is rather large for  $Mn_{15}$ . The present value is  $0.87 \mu_B/\text{atom}$ , whereas the corresponding experimental value is  $1.66 \pm 0.02 \mu_B/\text{atom}$ . We have also found several isomers (Table I), but none of them are close to the experimental value. The ground state and all the closely lying isomers within  $\sim 0.1$  eV energy spacing are of derived icosahedral structure. The two competing icosahedral structures with  $5,1,5,1,3$  and  $1,5,1,5,1,2$  staking (i.e. without or with the apex atom) are possible (Fig.3). The first kind of structure is found to be the ground state, whereas the optimal structure for the second kind lies  $0.06$  eV higher with a magnetic moment  $13 \mu_B$  (Fig.3). Another structure of the second kind is found to be degenerate with this isomer, which has a magnetic moment  $7 \mu_B$  (Table I). However, using US-PP Briere *et al.* found a bcc structure to be the ground state with much smaller magnetic moment,  $0.20 \mu_B/\text{atom}$ <sup>21</sup>. In the present case this bcc kind of structure lies  $0.28$  eV higher (Table I).

The same structural trend is observed in the case of  $Mn_{16}$ , the two different competing geometries have been found to be the possible candidates for the  $Mn_{16}$  cluster. Both of these structures can be derived from the 19-atom double icosahedra, which has a  $1,5,1,5,1,5,1$ -atomic staking. The ground state has a magnetic moment  $1.25 \mu_B/\text{atom}$  with  $N_\uparrow = 9$  spin structure. This structure has  $5,1,5,1,4$ -atomic staking: both the apex atoms and one atom from the lower pentagonal ring are missing from the double icosahedra. The next isomer has the same atomic arrangement and is almost degenerate, which lies only  $0.02$  eV higher. This has  $1.38 \mu_B/\text{atom}$  magnetic moment and the same ( $N_\uparrow = 9$ ) spin ordering. For both of these structures the central pentagonal ring is antiferromagnetically coupled with the upper and lower (incomplete) pentagonal ring. The experimentally predicted value,  $1.58 \pm 0.02 \mu_B$ <sup>3,4</sup> is very close to these predicted values and confirms the corresponding ground state to be really of this ‘strange’ staking. The next two isomers have a different icosahedral geometry and have comparatively smaller magnetic moment,  $0.63$  (Fig. 3) and  $0.50 \mu_B/\text{atom}$ . They lie  $0.06$  and  $0.1$  eV higher,

TABLE I: Binding energy, relative energy to the GS ( $\Delta E = E - E_{GS}$ ), magnetic moment (with a comparison to the SG experiment<sup>3,4</sup>) and different spin gaps,  $\Delta_1$  and  $\Delta_2$ , for  $Mn_n$  ( $n = 2-20$ ) clusters.

Cluster	$E_b$ (eV/atom)	$\Delta E$ (eV)	Magnetic Moment ( $\mu_B$ /atom)				Spin Gaps (eV)	Cluster	$E_b$ (eV/atom)	$\Delta E$ (eV)	Magnetic Moment ( $\mu_B$ /atom)				Spin Gaps (eV)
			Theory		SG	Exp. <sup>3,4</sup>					Theory		SG	Exp. <sup>3,4</sup>	
														$\delta_1$	$\delta_2$
$Mn_2$	0.52	0.00	5.00	—	0.95	1.31		$Mn_{12}$	2.08	0.00	1.33	$1.72 \pm 0.04$	0.48	0.26	
	0.26	0.52	0.00	—	0.47	0.47			2.08	0.05	0.33	0.40	0.30		
$Mn_3$	0.82	0.00	5.00	—	0.73	1.27		$Mn_{13}$	2.07	0.11	1.50	0.05	0.45		
	0.81	0.05	1.67	—	0.63	0.58			2.17	0.00	0.23	$0.54 \pm 0.06$	0.34	0.38	
$Mn_4$	1.18	0.00	5.00	—	0.66	2.35		$Mn_{14}$	2.16	0.08	0.54	0.36	0.20		
	1.16	0.08	2.50	—	0.45	0.85			2.17	0.00	1.29	$1.48 \pm 0.03$	0.23	0.24	
	1.13	0.20	0.00	—	0.41	0.41			2.17	0.02	1.43	0.24	0.31		
	1.13	0.20	2.00	—	1.12	0.21			2.17	0.05	1.57	0.25	0.32		
$Mn_5$	1.41	0.00	0.60	$0.79 \pm 0.25$	1.03	0.30		$Mn_{15}$	2.23	0.00	0.87	$1.66 \pm 0.02$	0.36	0.27	
	1.40	0.06	2.60	—	0.97	0.37			2.23	0.03	0.33	0.16	0.29		
	1.40	0.07	1.00	—	0.16	0.65			2.23	0.06	0.47	0.20	0.23		
	1.37	0.19	4.60	—	0.55	0.77			2.23	0.06	0.87	0.27	0.36		
$Mn_6$	1.57	0.00	1.33	$0.55 \pm 0.10$	0.48	0.35		$Mn_{16}$	2.23	0.06	1.00	0.25	0.45		
	1.56	0.02	0.33	—	0.40	0.31			2.21	0.28	0.47	0.39	0.35		
	1.56	0.05	2.67	—	0.86	0.32			2.27	0.00	1.25	$1.58 \pm 0.02$	0.33	0.22	
	1.54	0.14	4.33	—	0.98	1.16			2.27	0.02	1.38	0.19	0.52		
$Mn_7$	1.73	0.00	0.71	$0.72 \pm 0.42$	0.45	0.65		$Mn_{17}$	2.27	0.06	0.63	0.28	0.35		
	1.71	0.09	1.00	—	0.56	0.23			2.27	0.10	0.50	0.30	0.20		
$Mn_8$	1.70	0.19	0.43	—	0.51	0.13		$Mn_{18}$	2.33	0.00	1.59	$1.44 \pm 0.02$	0.25	0.37	
	1.77	0.00	1.00	$1.04 \pm 0.14$	0.61	0.20			2.32	0.08	1.47	0.25	0.09		
	1.77	0.00	1.50	—	0.40	0.41			2.32	0.09	1.71	0.14	0.70		
$Mn_9$	1.77	0.04	1.25	—	0.35	0.25		$Mn_{19}$	2.35	0.00	1.67	$1.20 \pm 0.02$	0.36	0.30	
	1.87	0.00	0.78	$1.01 \pm 0.10$	0.49	0.36			2.35	0.02	1.56	0.34	0.33		
	1.86	0.10	1.44	—	0.24	0.60			2.35	0.02	1.44	0.35	0.25		
$Mn_{10}$	1.85	0.15	0.78	—	0.30	0.34		$Mn_{20}$	2.35	0.06	1.78	0.18	0.55		
	1.84	0.21	1.00	—	0.24	0.36			2.37	0.00	1.10	$0.41 \pm 0.04$	0.19	0.22	
	1.94	0.00	1.40	$1.34 \pm 0.09$	0.27	0.44			2.37	0.01	1.00	0.24	0.16		
	1.94	0.01	1.00	—	0.69	0.13			2.37	0.08	0.47	0.22	0.15		
$Mn_{11}$	1.94	0.01	0.40	—	0.36	0.41			2.37	0.00	1.40	$0.93 \pm 0.03$	0.39	0.19	
	1.94	0.01	0.40	—	0.37	0.20			2.37	0.00	1.50	0.21	0.20		
	1.99	0.00	0.82	$0.86 \pm 0.07$	0.26	0.29			2.37	0.05	1.60	0.12	0.35		
	1.98	0.11	0.46	—	0.34	0.20			2.37	0.07	0.80	0.30	0.21		
	1.98	0.15	0.64	—	0.10	0.45			2.37						

respectively. Both of them have 1,5,1,5,1,3 staking, i.e. the 13-atom icosahedra is complete. The two complete pentagonal rings are antiferromagnetically coupled. All these structures have same number of  $N_\uparrow$  and  $N_\downarrow$  but have two different class of atomic arrangements, which is consequently the reason for their large difference in the magnetic moment.

The  $Mn_{17}$  cluster follows the same structural trend seen in both  $Mn_{15}$  and  $Mn_{16}$ . The ground state is a double icosahedra without both the apex atoms, i.e. it has 5,1,5,1,5 staking. The spin structure is  $N_\uparrow = 10$  and the central pentagonal ring is AFM coupled with the other rings. This structure has a magnetic moment of 1.59  $\mu_B$ /atom, which is in excellent agreement with the experiment,  $1.44 \pm 0.02 \mu_B$ /atom<sup>4</sup>. The next two isomers also have the same conformation as well as the same spin structure. For this size the structure of the second kind i.e. the icosahedral structure with one apex atom (Fig.3) lies rather higher in energy. To our knowledge, there is no available report for any other elements where this kind

of staking has been observed to be the ground state for  $Mn_{15} - Mn_{17}$  clusters.

The  $Mn_{18}$  is the 19-atom double icosahedra without one apex atom. The predicted magnetic moment is 1.67  $\mu_B$ /atom, whereas the experimental value is slightly smaller,  $1.20 \pm 0.02 \mu_B$ /atom<sup>4</sup>. Next two isomers are nearly degenerate and have 1.56 and 1.44  $\mu_B$ /atom magnetic moment (Table I). For all these structures the integrated magnetization densities  $\mathcal{M}$  for the central pentagonal bi-pyramid are negative (Fig. 3).

The double icosahedral conformation is found to be the ground state for  $Mn_{19}$ . The predicted magnetic moment is 1.10  $\mu_B$ /atom (Fig. 3), which is smaller than those of its neighboring clusters, what has been predicted by the experiment<sup>3,4</sup>. Another magnetic structure has been found to be degenerate with 1  $\mu_B$ /atom magnetic moment (not shown in Fig. 3). Both of the structures have  $N_\downarrow = 7$  and the central pentagonal ring is AFM coupled with the other two rings. However, the predicted magnetic moment is larger than the experimentally measured

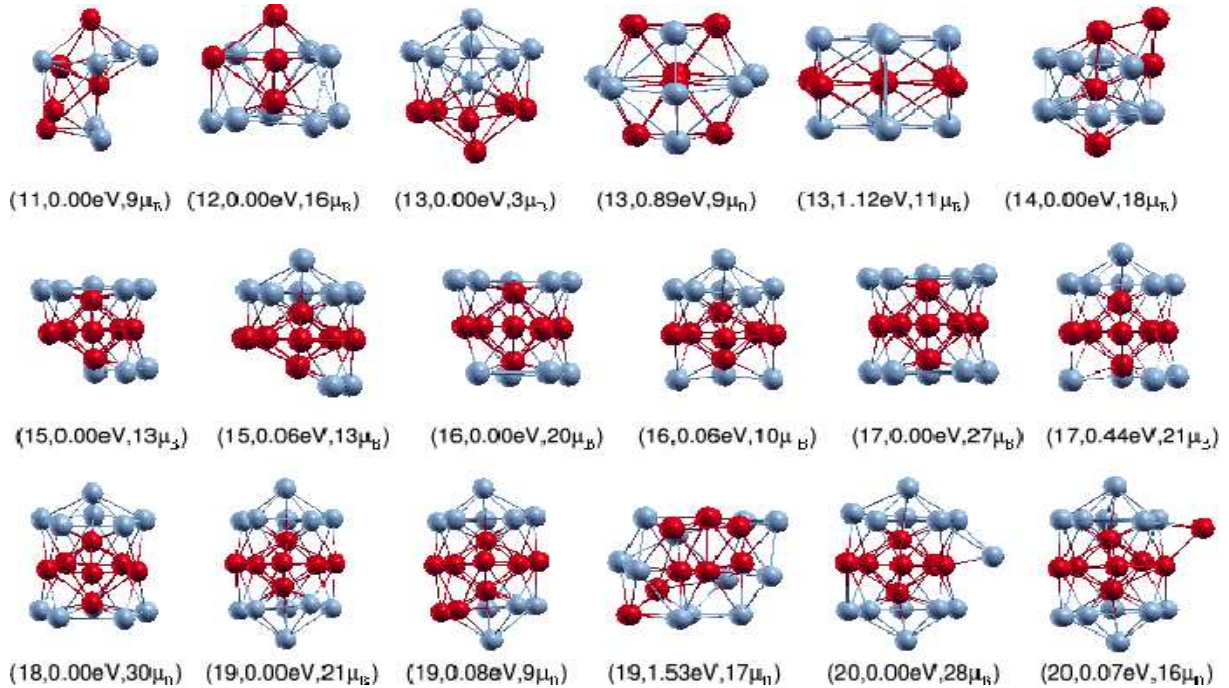


FIG. 3: (Color online) The ground state and a few higher energy structures for the size range  $n = 11 - 20$ . Note the grouping of the same kind of spins.

value,  $0.41 \pm 0.04 \mu_B/\text{atom}^4$ . In our case a magnetic structure with a magnetic moment  $0.47 \mu_B/\text{atom}$  ( $N_\downarrow = 9$ ), which is very close to the experimentally measured value, lies only  $0.08 \text{ eV}$  higher in energy (Fig 3). The optimal FCC structure lies much higher,  $1.53 \text{ eV}$ , in energy, which is shown in Fig. 3.

Two degenerate ground states have been found with  $1.40$  and  $1.50 \mu_B/\text{atom}$  magnetic moment for Mn<sub>20</sub> cluster. Both the structures have  $N_\downarrow = 7$  (Fig. 3) spin conformation and the conformation can be seen as a singly

capped 19-atom double icosahedra. The central pentagonal ring is antiferromagnetically coupled with the other two rings. The predicted ground state magnetic moment is larger than the experimental value,  $0.93 \pm 0.03 \mu_B/\text{atom}^4$ . However, a different spin structure ( $N_\downarrow = 8$ ) with magnetic moment  $0.80 \mu_B/\text{atom}$ , which is close to the experimentally predicted value, lies only  $0.07 \text{ eV}$  higher (Fig. 3).

In the intermediate size range, the grouping of like spin atoms i.e spin segregation occurs (Fig. 3). For a particular sized cluster, we find that the ferromagnetically aligned atoms have longer average bond lengths<sup>35</sup> than those of the antiferromagnetically aligned ones. This is because of the Pauli repulsion.

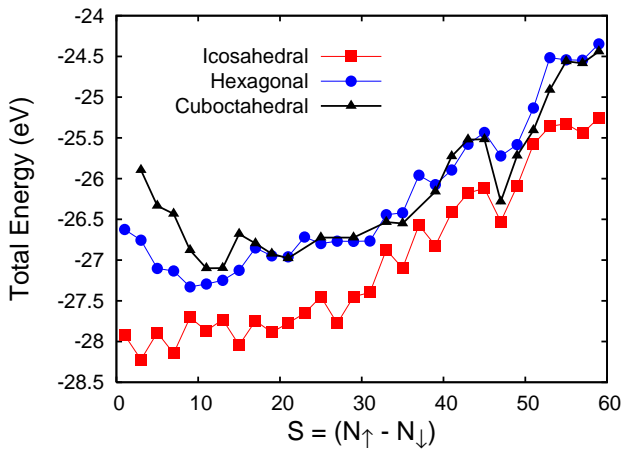


FIG. 4: (Color online) Plot of the total energy as a function of total magnetic moment  $S = (N_\uparrow - N_\downarrow)$  for icosahedral, hexagonal closed pack and cuboctahedral conformations for Mn<sub>13</sub> cluster.

#### D. Binding Energies

The size dependence of the ground state binding energy for Mn<sub>n</sub> clusters ( $n = 2-20$ ) is shown in Fig. 5. Due to the lack of hybridization between the half-filled 3d and filled 4s states and due to high  $4s^23d^5 \rightarrow 4s^13d^6$  promotion energy, the Mn<sub>2</sub> dimer is a weakly bound dimer, which is a characteristic of van der Waals bonding<sup>8,9,10</sup>. As the number of atoms in the cluster increases, the binding energy increases monotonically due to the increase in the  $s-d$  hybridization. However, it remains weak as compared to the other transition metal clusters in the same size range. This weak bonding has been demonstrated through the photodissociation experiments for Mn<sub>n</sub><sup>+</sup> ( $n \leq 7$ ) cluster cations<sup>11,12</sup>. Recently, we have shown<sup>36</sup> that if

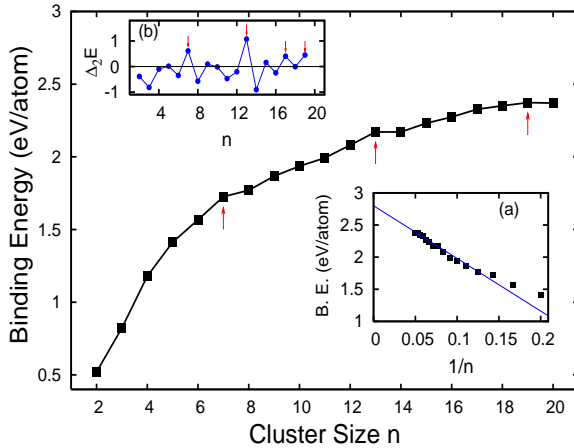


FIG. 5: (Color online) Plot of binding energy per atom as a function of cluster size  $n$  for the entire size range  $2 \leq n \leq 20$ . (a) Plot of the same as a function of  $1/n$  for the ferrimagnetic clusters,  $5 \leq n \leq 20$  and a linear fit ( $B.E. = -8.20\frac{1}{n} + 2.80$ ) to the data. (b) Plot of second difference,  $\Delta_2 E$  in energy, which represents the relative stability.

an As-atom is doped to the  $Mn_n$  clusters, the binding energies of the resultant  $Mn_nAs$  clusters increase substantially due to their hybridized  $s - d$  electrons bond with the  $p$  electrons of As. Similar enhancement in bonding has also been seen due to the single nitrogen doping<sup>37</sup>.

Upon extrapolation of the linear fit to the binding energy per atom data to  $1/n \rightarrow 0$  (Fig.5(a)), we obtained the binding energy for an infinitely large cluster as 2.80 eV, which is very close to the experimental AF bulk  $\alpha$ -Mn (2.92 eV). It is important here to note the kinks observed at  $n = 7$  and  $13$  in the binding energy curve (Fig.5). These kinks represent enhanced stability rendered by their ‘closed’ geometric structures:  $Mn_7$  is PBP and  $Mn_{13}$  is the first complete icosahedra. If this argument is valid then there should also be a kink at  $n = 19$ , due to the fact it has double icosahedral structure. But we do not see any prominent kink in the binding energy curve. So, it will be interesting to investigate the second difference in the binding energy,  $\Delta_2 E(n) = E(n+1) + E(n-1) - 2E(n)$ , where  $E(n)$  represents the total energy of an  $n$ -atom cluster. As  $\Delta_2 E(n)$  represents stability of the corresponding cluster compared to its neighbors, the effect will be prominent.  $\Delta_2 E$  is plotted in the Fig.5(b), where we see a peak for  $Mn_{19}$  too along with  $n = 7$  and  $13$ . However, in addition, without any a priory reason, we observe another peak at  $n = 17$ , which does not have ‘closed’ structure (a double icosahedra without two apex atoms).

### E. Transition in magnetic ordering

For very small clusters,  $n \leq 4$ , the magnetic coupling is found to be FM with magnetic moments  $5 \mu_B/\text{atom}$ , which is the Hund’s rule value for an isolated Mn atom.

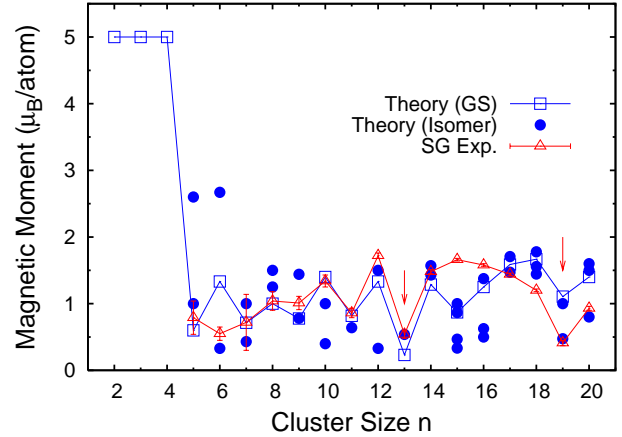


FIG. 6: (Color online) Size dependent variation of magnetic moment. For the size range  $5 \leq n \leq 20$ , it shows excellent agreement with the SG experiment. Isomers which lie very close to the corresponding GS energy are also shown.

Although we see that for  $Mn_3$  cluster the FM solution is nearly degenerate with the frustrated AFM solution. The size dependence of the magnetic moment per atom is plotted in the Fig.6. We see the transition in the magnetic coupling (from FM to ferrimagnetic) takes place at  $n = 5$  and the ferrimagnetic states continue to be the ground state for the entire size range  $n = 5-20$ . Fig.6 shows a very good agreement between experimentally measured and our predicted magnetic moments. It was seen in the SG experiment that the experimental uncertainty in measuring the magnetic moment decreases with the cluster size. However, this is not the case for  $Mn_7$ , for which the measured uncertainty is quite large ( $0.72 \pm 0.42 \mu_B$ ,  $\pm 58\%$  of the measured value) as compared to the neighbouring sizes. This large uncertainty might arise from the presence of isomers with different magnetic moments in the SG beam for subsequent measurements. However, in addition with the statistical fluc-

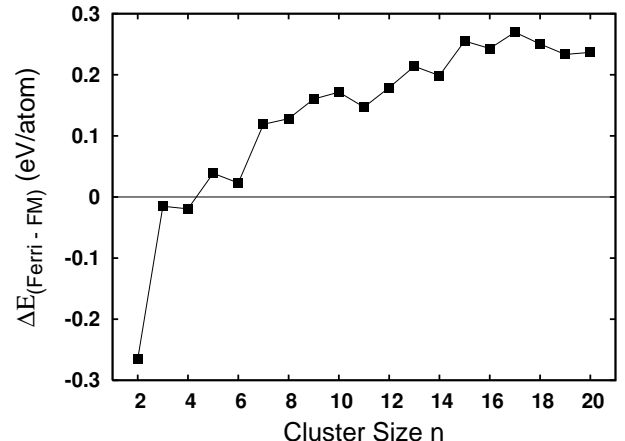


FIG. 7: Plot of  $\Delta E_{(\text{Ferri} - \text{FM})}$  as a function of cluster size  $n$ .

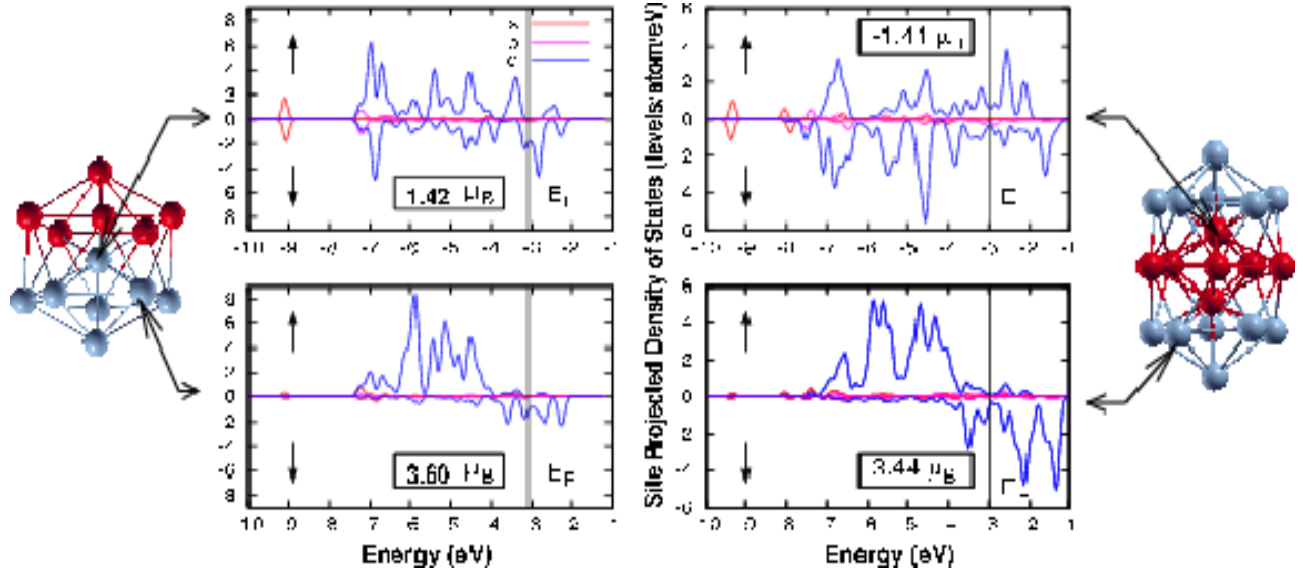


FIG. 8: (Color online) The  $s$ -,  $p$ - and  $d$ -projected density of states for the central and surface atoms for  $Mn_{13}$  and  $Mn_{19}$  in their ground state. Gaussian broadening of half-width 0.1 eV has been used. Integrated magnetization density  $\mathcal{M}$  for each atom is given in the box.

tuation, the above explanation only stands for a plausible reason as for all other sizes we did find many isomers with different magnetic moments (see Table I and Fig.6), but the corresponding experimental uncertainty is not that large. One another striking feature observed in the experiment is the sudden decrease in the magnetic moment at  $n=13$  and  $19$ , compared to their neighbors. Our calculation reproduces this feature. This is attributed to their ‘closed’ icosahedral structures: first complete icosahedra for  $Mn_{13}$  and a double icosahedra for  $Mn_{19}$ . The other geometries studied viz. hexagonal closed packed and cuboctahedral structures for  $Mn_{13}$  and a fcc structure for  $Mn_{19}$  lie much higher in energy, 0.89 eV ( $9 \mu_B$ ), 1.12 eV ( $11 \mu_B$ ) and 1.53 eV ( $17 \mu_B$ ), respectively, than their corresponding ground state.

In the Fig.6 we have depicted the magnetic moments of the very closely lying isomers with their ground state (see Table I) and while comparing those with the experimentally observed values, we come to the conclusion that for a particular size of cluster, the isomers with different magnetic moments are likely to be present in the SG cluster beam with a statistical weight and essentially, the measured moment is the weighted average of those isomers. We calculate the energy difference between the optimal FM and optimal ferrimagnetic solutions,  $\Delta E_{(\text{Ferri-FM})} = E(\text{Ferri}) - E(\text{FM})$ , and plot them as a function of cluster size  $n$  in the Fig.7. For both  $Mn_3$  and  $Mn_4$  the FM solutions are slightly lower in energy than those of their respective optimal ferrimagnetic solutions, whereas the optimal FM solutions are slightly higher than the corresponding ferrimagnetic ground states for  $Mn_5$  and  $Mn_6$ . Thereafter, as the cluster size increases, this energy difference,  $\Delta E_{(\text{Ferri-FM})}$ , increases almost monotonically indicating that the opti-

mal FM solutions become more and more unlikely. All these optimal FM states have  $\sim 4 \mu_B/\text{atom}$  magnetic moments.

#### F. Coordination and the $d$ -electron localization

The angular momentum projected local density of states (LDOS) show interesting site dependency. The  $s$ -,  $p$ - and  $d$ -projected LDOS for the central and surface atoms are plotted in the Fig.8 for the  $Mn_{13}$  and  $Mn_{19}$  clusters. We see only  $d$ -projected LDOS are significant and are of great interest here. The  $d$ -projected LDOS of both  $Mn_{13}$  and  $Mn_{19}$  for the central atoms are broad for both majority and minority spin states, which are also reflected through their small values of the integrated spin densities  $\mathcal{M}$  ( $1.42 \mu_B$  and  $-1.41 \mu_B$  for  $Mn_{13}$  and  $Mn_{19}$ , respectively). The broadening occurs due to the high coordination of the central atom. On the other hand, the  $d$ -projected LDOS of the surface atoms are rather localized and the majority spins are nearly fully occupied, which is in agreement with the relatively large local magnetic moments of the surface atoms ( $3.60 \mu_B$  and  $3.44 \mu_B$  for  $Mn_{13}$  and  $Mn_{19}$ , respectively).

#### G. Spin gaps: Nonmetal – metal transition?

A spin arrangement in any magnetic clusters is magnetically stable only if both the spin gaps,

$$\begin{aligned} \delta_1 &= - \left[ \epsilon_{\text{HOMO}}^{\text{majority}} - \epsilon_{\text{LUMO}}^{\text{minority}} \right] \\ \delta_2 &= - \left[ \epsilon_{\text{HOMO}}^{\text{minority}} - \epsilon_{\text{LUMO}}^{\text{majority}} \right], \end{aligned} \quad (3)$$

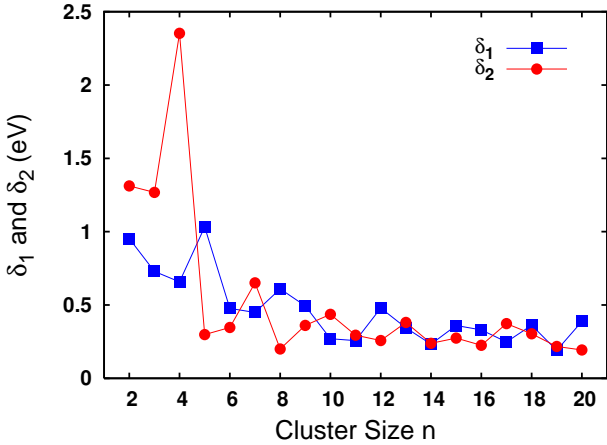


FIG. 9: (Color online) Plot of spin gaps as a function of cluster size  $n$ . See Table I for the numerical values.

are positive, i.e. the lowest unoccupied molecular orbital (LUMO) of the majority spin lies above the highest occupied molecular orbital (HOMO) of the minority spin and vice versa. We find these two spin gaps to be positive for all the clusters (Table I) discussed here and are plotted in the Fig.9.  $\delta_1$  and  $\delta_2$  have local structures, but generally decreases slowly as the coordination increases with cluster size. Parks *et al.* found that the  $Mn_n$  clusters with  $n \leq 15$  are not reactive towards molecular hydrogen, whereas they form stable hydrides at and above  $n = 16$ , and the reaction rate varies considerably with the cluster size<sup>22</sup>. They argued it to be attributed from the non-metal to metal transition at  $n = 16$ . If this is indeed the reason, it is likely that the ionization potential would show a significant decrease at  $Mn_{16}$ , similar to what has been observed for free mercury clusters<sup>38</sup>. Therefore, we expect closing up of the spin gaps at  $n = 16$ . However, Koretsky *et al.* observed no sudden decrease in the measured ionization potential<sup>23</sup> and we do not find any spin gap closing at  $Mn_{16}$  either. The spin gaps have reasonable value,  $\delta_1 = 0.33$  eV and  $\delta_2 = 0.22$  eV for  $Mn_{16}$  cluster (Fig.9 and Table I). This abrupt change in the reaction rate with  $H_2$  at  $Mn_{16}$  is not due to any structural change either, as we find all the medium sized clusters adopt icosahedral growth pattern and the reason for the observed change in the reaction rate remains unknown.

#### IV. SUMMARY AND CONCLUSIONS

We have systematically investigated the structural, electronic and magnetic properties of  $Mn_n$  ( $n = 2-20$ )

clusters from the first-principles density functional theory. An extensive search have been made to locate the global minima. Due to the intrinsic  $4s^2 3d^5$  electronic structure and high  $4s^2 3d^5 \rightarrow 4s^1 3d^6$  promotion energy Mn-atoms do not bind strongly when they come closer to form a cluster. However, binding energy increases with the cluster size as the coordination number increases and reaches a value 2.37 eV/atom for  $Mn_{20}$ , which is 81 % of the bulk value. A magnetic transition from FM to ferrimagnetic ordering takes place at  $n = 5$  and thereafter the energy difference between the optimal ferrimagnetic and optimal FM structure increases with the cluster size, which indicates that the optimal FM states become more and more unfavorable with increasing cluster size. However, different ferrimagnetic states are possible within a small  $\sim 0.1$  eV energy difference and their plausible presence in the experimental SG beam along with the ground state has been argued. The predicted magnetic moments are in agreement with the SG experiment. The sudden decrease in the magnetic moment at  $n = 13$  and 19 is due to their ‘closed’ icosahedral structure. It should be pointed out here that in the present calculation we assumed only collinear alignment of spins. However, spin canting or noncollinear magnetic ordering is possible in small magnetic clusters as it occurs more easily in a low symmetry magnetic system<sup>36</sup>. Icosahedral growth pattern is observed for the intermediate size range. However, to our knowledge, a different kind of icosahedral packing have been observed for  $Mn_{15} - Mn_{17}$  clusters. In any particular cluster, the average bond length between antiferromagnetically aligned atoms are 3–8 % shorter than that of the ferromagnetically aligned, which can be explained in terms of the Pauli repulsion. Spin segregation has been observed in the intermediate size range. The  $d$ –electron localization strongly depends on coordination: localization decreases with the coordination number. There is no signature of non-metal to metal transition at  $n = 16$ , which has been predicted<sup>22</sup> through the downward discontinuity observed in the reaction rate with  $H_2$ .

#### Acknowledgments

We are grateful to Dr. P. A. Sreeram for helpful discussions. This work has been done under the Indian Department of Science and Technology grant No. SR/S2/CMP-25/2003. M. K. thankfully acknowledges the congenial hospitality at the Centre for Modeling and Simulation of Pune University. We also acknowledge the DST grant No. SP/S2/M-20/2001 for using computational resource.

<sup>1</sup> A. J. Cox, J. G. Louderback and L. A. Bloomfield, Phys. Rev. Lett. **71**, 923 (1993); A. J. Cox, J. G. Louderback, S. E. Apsel and L. A. Bloomfield, Phys. Rev. B **49**, 12295

(1994).  
<sup>2</sup> L. A. Bloomfield, J. Deng, H. Zhang and J. W. Emmert, in *Proceedings of the International Symposium on Cluster and*

*Nanostructure Interfaces*, edited by P. Jena, S. N. Khanna and B. K. Rao (World Publishers, Singapore, 2000), p.131

<sup>3</sup> M. B. Knickelbein, Phys. Rev. Lett. **86**, 5255 (2001).

<sup>4</sup> M. B. Knickelbein, Phys. Rev. B **70**, 14424 (2004).

<sup>5</sup> I. M. L. Billas, J. A. Becker, A. Châtelain and W. A. de Heer, Phys. Rev. Lett. **71**, 4067 (1993); D. M. Cox, D. J. Trevor, R. L. Wheatten, E. A. Rohlffing and A. Kaldor, Phys. Rev. B **32**, 7290 (1985).

<sup>6</sup> Xiaoshan Xu, Shuangye Yin, Ramiro Moro and Walt A. de Heer, Phys. Rev. Lett. **95**, 237209 (2005).

<sup>7</sup> C. E. Moore, *Atomic Energy Levels*, Natl. Bur. Stand. (U. S.) Circ. No. 467 (U. S. GPO, Washington, D. C., 1952), Vol. II.

<sup>8</sup> M. D. Morse, Chem. Rev. (Washington, D. C.) **86**, 1049 (1986).

<sup>9</sup> K. A. Gingerich, Faraday Discuss. Chem. Soc. **14**, 109 (1980).

<sup>10</sup> A. Kant, S.-S. Lin and B. Strauss, J. Chem. Phys. **49**, 1983 (1968).

<sup>11</sup> A. Terasaki, S. Minemoto and T. Kondow, J. Chem. Phys. **117**, 7520 (2002).

<sup>12</sup> K. Tono, A. Terasaki, T. Ohta and T. Kondow, J. Chem. Phys. **123**, 174314 (2005).

<sup>13</sup> R. J. Van Zee and W. Weltner,Jr., J. Chem. Phys. **89**, 4444 (1988); C. A. Bauman, R. J. Van Zee, S. Bhat, and W. Weltner,Jr., J. Chem. Phys. **78**, 190 (1983).

<sup>14</sup> S. K. Nayak, B. K. Rao and P. Jena, J. Phys.: Condens. Matter **10**, 10863 (1998).

<sup>15</sup> S. K. Nayak and P. Jena, Chem. Phys. Lett. **289**, 473 (1998).

<sup>16</sup> M. R. Pederson, F. Ruse and S. N. Khanna, Phys. Rev. B **58**, 5632 (1998).

<sup>17</sup> S. K. Nayak, M. Nooijen and P. Jena, J. Phys. Chem. A **103**, 9853 (1999).

<sup>18</sup> P. Bobadova-Parvanova, K. A. Jackson, S. Srinivas and M. Horoi, Phys. Rev. A **67**, 61202(R) (2003).

<sup>19</sup> P. Bobadova-Parvanova, K. A. Jackson, S. Srinivas and M. Horoi, J. Chem. Phys. **122**, 14310 (2005).

<sup>20</sup> N. O. Jones, S. N. Khanna, T. Baruah and M. R. Pederson, Phys. Rev. B **70**, 45416 (2004).

<sup>21</sup> T. M. Briere, M. H. F. Sluiter, V. Kumar and Y. Kawazoe, Phys. Rev. B **66**, 64412 (2002).

<sup>22</sup> E. K. Parks, G. C. Nieman and S. J. Riley, J. Chem. Phys. **104**, 3531 (1996).

<sup>23</sup> G. M. Koretsky and M. B. Knickelbein, J. Chem. Phys. **106**, 9810 (1997).

<sup>24</sup> P. E. Blöchl, Phys. Rev. B **50**, 17953 (1994).

<sup>25</sup> G. Kresse and D. Joubert, Phys. Rev. B **59**, 1758 (1999).

<sup>26</sup> J. P. Perdew, K. Burke and M. Ernzerhof, Phys. Rev. Lett. **77**, 3865 (1996).

<sup>27</sup> G. Kresse and J. Furthmüller, Phys. Rev. B **54**, 11169 (1996).

<sup>28</sup> K. D. Bier, T. L. Haslett, A. D. Krikwood and M. Moskovits, J. Chem. Phys. **89**, 6 (1988).

<sup>29</sup> R. J. Van Zee, C. A. Baumann and W. Weltner, J. Chem. Phys. **74**, 6977 (1981).

<sup>30</sup> M. F. Jarrold, A. J. Illies and M. T. Bowers, J. Am. Chem. Soc. **107**, 7339 (1985).

<sup>31</sup> G. W. Ludwig, H. H. Woodbury and R. O. Carlson, J. Phys. Chem. Solids **8**, 490 (1959).

<sup>32</sup> S. N. Khanna, B. K. Rao, P. Jena and M. B. Knickelbein, Chem. Phys. Lett. **378**, 374 (2003).

<sup>33</sup> M. Kabir, A. Mookerjee and A. K. Bhattacharya, Eur. Phys. J. D **31**, 477 (2004).

<sup>34</sup> M. Kabir, A. Mookerjee and A. K. Bhattacharya, Phys. Rev. A **69**, 043203 (2004).

<sup>35</sup> The average bond lengths were calculated by assuming a cut-off of 3 Å.

<sup>36</sup> M. Kabir, D. G. Kanhere and A. Mookerjee, Phys. Rev. B **73**, 75210 (2006).

<sup>37</sup> B. K. Rao and P. Jena, Phys. Rev. Lett. **89**, 185504 (2002).

<sup>38</sup> K. Rademann, B. Kaiser, U. Even, and F. Hensel, Phys. Rev. Lett. **59**, 2319 (1987).